0888-8809/07/$15.00/0
*Printed in U.S.A.*

Molecular Endocrinology 21(5):1049–1065

doi: 10.1210/me.2006-0485

# Impaired Peroxisome Proliferator-Activated Receptor $\gamma$ Function through Mutation of a Conserved Salt Bridge (R425C) in Familial Partial Lipodystrophy

Ellen H. Jeninga, Olivier van Beekum, Aalt D. J. van Dijk, Nicole Hamers, Brenda I. Hendriks-Stegeman, Alexandre M. J. J. Bonvin, Ruud Berger, and Eric Kalkhoven

*Department of Metabolic and Endocrine Diseases (E.H.J., O.v.B., N.H., B.I.H.-S., R.B., E.K.), University Medical Center Utrecht, 3584 EA Utrecht, The Netherlands; and Bijvoet Center for Biomolecular Research (A.D.J.v.D., A.M.J.J.B.), Utrecht University, 3584 CH Utrecht, The Netherlands*

**The nuclear receptor peroxisome proliferator-activated receptor (PPAR) $\gamma$ plays a key role in the regulation of glucose and lipid metabolism in adipocytes by regulating their differentiation, maintenance, and function. A heterozygous mutation in the *PPARG* gene, which changes an arginine residue at position 425 into a cysteine (R425C), has been reported in a patient with familial partial lipodystrophy subtype 3 (FPLD3). The strong conservation of arginine 425 among nuclear receptors that heterodimerize with retinoic acid X receptor prompted us to investigate the functional consequences of the R425C mutation on PPAR$\gamma$ function. Here we show that this mutant displayed strongly reduced transcriptional activity compared with wild-type PPAR$\gamma$, irrespective of cell type, promoter context, or ligand, whereas transrepression of nuclear factor-$\kappa$B activity remained largely intact. Our data indicate that the reduced transcriptional activity of PPAR$\gamma$ R425C is not caused by impaired corepressor release, but due to reduced dimerization with retinoic acid X receptor $\alpha$ in combination with reduced ligand binding and subsequent coactivator binding. As a consequence of these molecular defects, the R425C mutant was less effective in inducing adipocyte differentiation. PPAR$\gamma$ R425C did not inhibit its wild-type counterpart in a dominant-negative manner, suggesting a haploinsufficiency mechanism in at least some FPLD3 patients. Using molecular dynamics simulations, substitution of R425 with cysteine is predicted to cause the formation of an alternative salt bridge. This structural change provides a likely explanation of how mutation of a single conserved residue in a patient with FPLD3 can disrupt the function of the adipogenic transcription factor PPAR$\gamma$ on multiple levels. (*Molecular Endocrinology* 21: 1049–1065, 2007)**

THE PREVALENCE OF obesity and overweight rapidly increases worldwide (1). This is a major health concern, because adiposity is highly associated with insulin resistance, type 2 diabetes, dyslipidemia, hypertension, and atherosclerosis (components of the metabolic syndrome). Interestingly, the selective loss of adipose tissue (lipodystrophy) is also frequently associated with marked insulin resistance and complications such as type 2 diabetes, dyslipidemia, and hypertension (2). Thus, normal amounts of adipose tissue and normal fat distribution appear to be critical for the optimal regulation of lipid and energy metabolism.

Lipodystrophies represent a heterogeneous group of diseases characterized by altered amounts and/or distribution of body fat and major metabolic complications. The main forms can be classified according to their origin, either genetic or acquired, and subclassified according to the clinical pattern (3, 4). Whereas acquired lipodystrophies, like the metabolic syndrome and lipodystrophy due to highly active antiretroviral therapy (5) are fairly common, inherited forms of lipodystrophy are rare. Familial partial lipodystrophy (FPLD) is an autosomal dominantly inherited disorder, characterized by gradual loss of sc fat from the extremities and an accumulation of excess fat in the intraabdominal regions (3, 4). FPLD subtype 3 (FPLD3, MIM 604367) is associated with mutations in the peroxisome proliferator-activated receptor-$\gamma$ (*PPARG*) gene (MIM 601487) (6, 7). The majority of FPLD3 pa-

**First Published Online February 20, 2007**

Abbreviations: CBP, cAMP response element binding protein-binding protein; DBD, DNA binding domain; FPLD, familial partial lipodystrophy; GST, glutathione-*S*-transferase; ID1, interaction domain 1; LBD, ligand binding domain; NF-$\kappa$B, nuclear factor-$\kappa$B; PPAR, peroxisome proliferator-activated receptor; *PPARG*, PPAR-$\gamma$ gene; PPREs, PPAR-responsive elements; RTH, resistance to thyroid hormone; RXR, retinoic acid X receptors; SMRT, silencing mediator for retinoid and thyroid-hormone receptors; SRC, steroid receptor coactivator; TR$\beta$, thyroid hormone receptor $\beta$; TZDs, thiazolidinediones; VP16, viral protein 16 of herpes simplex virus.

***Molecular Endocrinology* is published monthly by The Endocrine Society (http://www.endo-society.org), the foremost professional society serving the endocrine community.**

tients have profound metabolic disorders, in particular severe insulin resistance and early onset diabetes mellitus, with polycystic ovarium syndrome seen in female subjects as a direct consequence of insulin resistance and marked or extreme dyslipidemia, characterized by high triglycerides and low high-density lipoprotein cholesterol. Some subjects also suffer from hypertension and hepatic steatosis (6, 7).

The *PPARG* gene encodes the PPARγ protein, a member of the nuclear receptor superfamily of ligand inducible transcription factors (8–10). Differential promoter usage and alternative splicing of the PPARγ gene generates four mRNA species (PPARγ 1–4), but just two different receptor proteins, PPARγ1 and PPARγ2. The PPARγ2 isoform contains 28 additional amino acids at its N terminus and its expression is restricted to adipose tissue, whereas PPARγ1 is more widely expressed (*e.g.* in adipose tissue, lower intestine, and macrophages). PPARγ plays a key role in glucose and lipid metabolism in adipocytes (8–10). Studies in murine cell lines have established that liganded PPARγ is both essential and sufficient for adipogenesis (11), whereas PPARγ knockout mice fail to develop adipose tissue (12–14). In addition, PPARγ directly regulates the expression of a number of genes involved in net lipid partitioning into mature adipocytes. Besides PPARγ, two closely related receptors have been identified, named PPARα and PPARβ/δ, which are encoded by different genes (10, 15). These three related receptors all bind to the PPAR-responsive elements (PPREs) in the promoter regions of target genes as obligate heterodimers with retinoic acid X receptors (RXRs) but exhibit different physiological roles due to their distinct expression patterns and specific activation by different ligands. Like other nuclear receptors, PPARγ consists of distinct functional domains including a constitutively active transactivation domain (AF-1), at the N terminus, a centrally located highly conserved DNA binding domain (DBD) composed of two zinc finger motifs, and a C-terminal ligand binding domain (LBD) that contains a powerful ligand-dependent transactivation function (AF-2). Ligand binding stabilizes the active conformation of the PPARγ LBD, thereby serving as a molecular switch between activation and repression functions of the receptor (16, 17). On some promoters, unliganded PPARγ recruits corepressors like nuclear receptor corepressor and SMRT (silencing mediator for retinoid and thyroid-hormone receptors), which are part of multiprotein complexes containing histone deacetylase activity that repress gene transcription (18–20). Upon ligand binding, these corepressor complexes are released and replaced by coactivator complexes, including the steroid receptor coactivator (SRC) 1/cAMP response element binding protein-binding protein (CBP) and TRAP (thyroid hormone receptor-associated proteins)/DRIP (vitamin D receptor interacting proteins)/ARC (activator-recruited cofactor) complexes, that are involved in transcriptional activation (21, 22). The endogenous ligands for PPARγ are not firmly established although some natural compounds, like polyunsaturated fatty acids and prostaglandin J2 derivatives (15-deoxy-$\Delta^{12,14}$-PGJ2) have been shown to be able to activate PPARγ (23) (24). Synthetic PPARγ agonists include the thiazolidinediones (TZDs) (25) and tyrosine-based agonists (26), which ameliorate insulin resistance and lower blood glucose levels in patients with type 2 diabetes (8). At least part of this response is thought to occur through indirect regulation of gene expression by PPARγ, *e.g.* by transrepression of TNFα-induced nuclear factor-κB (NF-κB) activity (27, 28).

Seven PPARγ missense mutations have been described in patients suffering from FPLD3, which are located either in the DBD [C142R, C159Y, C190W (PPARγ2 nomenclature)] or in the LBD [V318M, F388L, R425C, P495L (PPARγ2 nomenclature)] (29–32). In addition, two nonsense mutations (R385X, Y355X) and two frameshift/premature stop mutations have been reported (32–34). Except for R425C, all mutations have been shown to result in receptors with reduced transcriptional activity and some, but not all mutants inhibited their wild-type counterpart in a dominant-negative manner (see also *Discussion*). The functional consequences of the R425C FPLD3-associated missense mutation, which changes arginine 425 into cysteine, are currently unknown. Interestingly, a structure-based sequence alignment of nuclear receptors revealed that this arginine residue is part of a structural signature, which defines nuclear receptors that form heterodimers with RXRα, including the thyroid hormone receptor β (TRβ) (35). Within this subclass of proteins, named class II receptors, R425 is involved in the formation of a conserved salt bridge with a negatively charged residue in helix 4/5 (E352 in PPARγ2). In contrast, the homodimeric class I receptors lack this conserved arginine residue and the internal salt bridge (35).

The strong conservation of arginine 425 in PPARγ2 among class II nuclear receptors together with the lack of functional data on the natural R425C mutation motivated us to investigate the functional consequences of this FPLD3-associated mutant. Here we combine detailed molecular analysis with structural modeling, using molecular dynamics simulations, to show that the R425C mutation found in a patient with FPLD3 causes aberrant salt bridge formation and thereby abrogates PPARγ transcriptional activity leading to an inhibition of adipocyte differentiation.

## RESULTS

### The FPLD3-Associated PPARγ2 R425C Displays Reduced Transcriptional Activity

As a first step in our analysis of the FPLD3-associated R425C mutation, its effect on the ability of PPARγ2 to activate transcription was tested in reporter assays. For this, the human osteosarcoma cell line U2OS was

used, which lacks endogenous PPARγ expression and displayed the most significant reporter activation by liganded PPARγ among several human cell lines tested. Cells were transfected with expression vectors encoding wild-type PPARγ2 or R425C mutant together with a reporter construct containing three copies of the PPRE found in the rat acyl coenzyme A promoter (36). Whereas wild-type PPARγ2 readily activated this 3xPPRE-tk-Luc reporter approximately 120-fold upon addition of the synthetic ligand rosiglitazone (1 μM), PPARγ2 R425C only activated this reporter 20-fold (Fig. 1A). Figure 1B shows that PPARγ2 R425C was functionally defective at all concentrations of rosiglitazone tested, including saturating amounts. Cotransfection with RXRα did not increase the transcriptional activity of either wild-type or mutant PPARγ, indicating that RXRα is not limiting under these experimental conditions (data not shown). Similar results were obtained in 293T cells, indicating that the reduced activity of the R425C mutant is not cell type specific (data not shown).

Because PPARγ can be activated by various ligands (23–26), reporter assays were also performed using several other synthetic and one natural PPARγ ligand. All the TZDs tested (rosiglitazone, pioglitazone, troglitazone, and ciglitazone) and the natural ligand 15-deoxy-$\Delta^{12,14}$-$PGJ_2$ showed similar differences in transcriptional activity between wild-type and mutant PPARγ2 (Fig. 1C). Interestingly, the impaired activity of the R425C mutant was partially restored by the tyrosine-based agonist GW1929, a strong agonist that is also capable of activating the FPLD3-associated V318M and P495L mutants of PPARγ2 (37).

The reporter construct used above contains three copies of a functional PPRE. To test the effect of PPARγ2 R425C on a more natural promoter, reporter assays were performed using a luciferase reporter construct containing the promoter of the human adipose aquaporin gene (*AQP7*), which contains a single functional PPRE (38). As shown in Fig. 1D, activation of this reporter by wild-type PPARγ2 was less pronounced (6- and 12-fold in the absence and presence of rosiglitazone, respectively), compared with the 3xPPRE reporter (Fig. 1A). However, mutation of R425 into cysteine reduced the ability of PPARγ2 to activate this natural promoter in a similar fashion (Fig. 1D).

Amino acid sequence alignment of PPARs revealed that the arginine at position 425 in PPARγ2 lies within a region that is highly conserved between species and different PPAR family members (Fig. 2A). To investigate the effect of the R425C mutation on other PPAR isoforms, analogous mutations were generated in PPARγ1 (R397C), PPARα (R388C), and PPARβ/δ (R361C) and the proteins were subsequently tested for

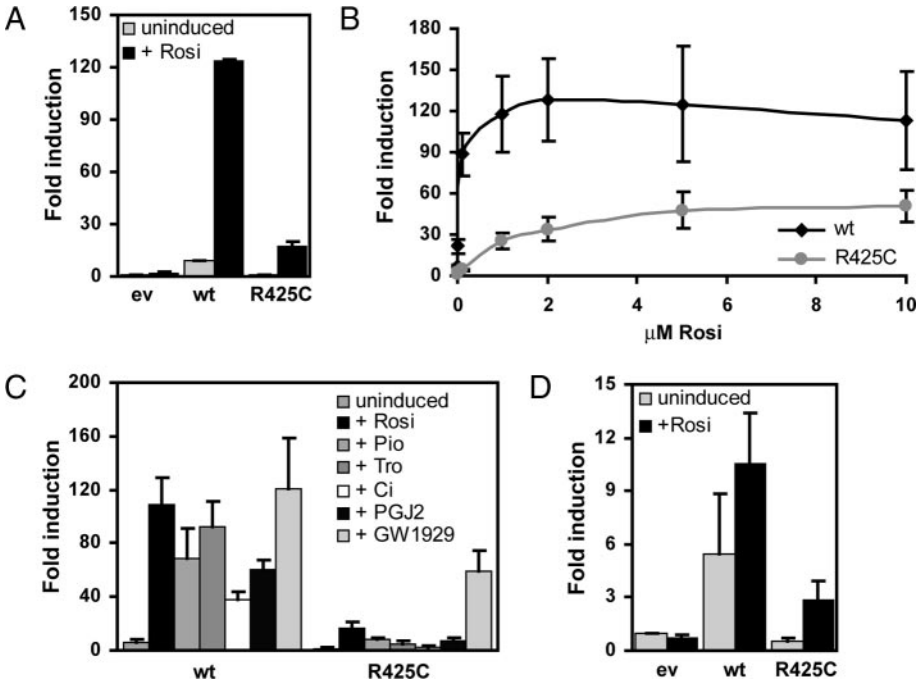


**Fig. 1.** The FPLD3-Associated R425C Mutation Reduces the Transcriptional Activity of PPARγ2

A, U2OS cells were transfected with expression vector encoding PPARγ2 wild-type (wt) or PPARγ2 R425C respectively, and a 3XPPRE-tk-Luc reporter. Activation of the luciferase reporter, in the absence or presence of 1 μM rosiglitazone (Rosi), is expressed as fold induction over that with empty vector (ev) in the absence of ligand, after normalization for *Renilla* luciferase activity. Results are averages of at least three independent experiments assayed in duplicate ± SEM. B, Dose-response curve of U2OS cells transfected as in panel A. C, Reporter assay as outlined in panel A using the PPARγ ligands, pioglitazone (Pio; 2 μM), troglitazone (Tro; 1.5 μM), ciglitazone (Ci; 6 μM), 15-deoxy-$\Delta^{12,14}$-$PGJ_2$ (PGJ2; 14 μM), and GW1929 (1 μM), respectively. D, U2OS cells were transfected as in A, but with the human adipose aquaporin (*AQP7*)-Luc reporter instead of the 3xPPRE-tk-Luc reporter.

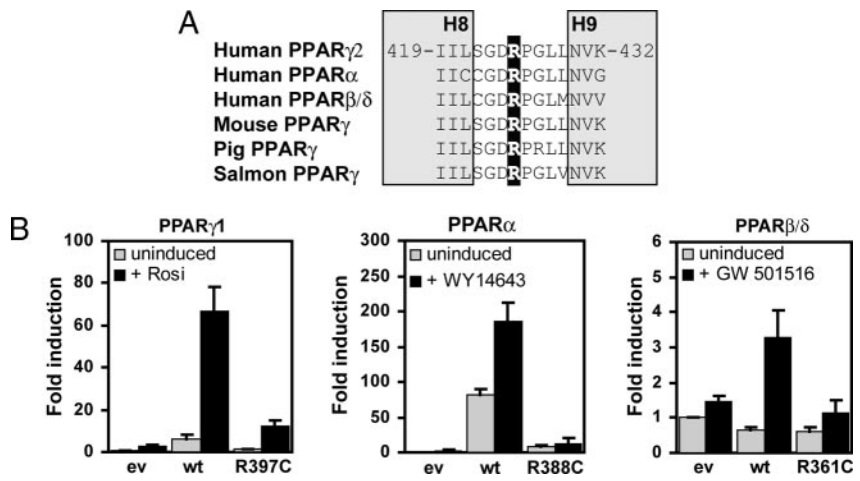


**Fig. 2.** Mutations Analogous to R425C in PPARγ2 Have Similar Effects on Transcriptional Activity of Different PPAR Proteins

A, Alignment of the amino acid sequence surrounding R425 in human PPARγ2 (CAA62153), with human PPARα (AAB32649), human PPARβ/δ (AAH02715), mouse PPARγ (AAO45098), pig PPARγ (CAA07225), and salmon PPARγ (CAC02968). Species in which the sequence surrounding R425 was identical with human and mouse [*e.g.* rat (AADA0119), zebrafish (AAY85274), *Xenopus* (AAH60474), chicken (AAL85323)] were omitted for reasons of clarity. Also indicated are the boundaries of helix 8 and 9, as defined in the crystal structure of the PPARγ LBD (17). B, U2OS cells were transfected with expression vectors encoding PPARγ1 wt or R397C mutant (*left panel*), PPARα or R388C mutant (*middle panel*) or PPARδ or R361C mutant (*right panel*). Activation of the 3xPPRE-tk-Luc reporter in the absence or presence of rosiglitazone (Rosi; 1 μM) for PPARγ1, WY14643 (100 μM) for PPARα, or GW501516 (2.2 nM) for PPARδ, are presented as described in Fig. 1A. ev, Empty vector; wt, wild type.

their ability to activate a 3xPPRE reporter construct in U2OS cells. Wild-type PPARγ1 activated the 3xPPRE-tk-Luc reporter approximately 70-fold upon addition of rosiglitazone, whereas the R397C mutant only activated this reporter 15-fold (Fig. 2B, *left panel*). As reported earlier (39), wild-type PPARα displayed significant activity in the absence of ligand, which was further increased by addition of the synthetic PPARα-specific ligand WY14643. Mutation of PPARα R388 into cysteine almost completely inhibited transcriptional activity, both in the absence and presence of ligand (Fig. 2B, *middle panel*). Finally, assays performed with PPARβ/δ showed that this receptor also activated the reporter upon addition of a specific PPARβ/δ ligand (GW501516), albeit significantly less than the PPARγ isoforms or PPARα. Nevertheless, the weak transcriptional activity of PPARβ/δ was clearly inhibited by mutating R361 into cysteine (Fig. 2B, *right panel*).

Collectively, these results suggest that the FPLD3-associated R425C mutation results in reduced transcriptional activity of PPARγ2, independent of ligand type, ligand concentration and promoter used. Furthermore, the reduced transcriptional activity of R425C is not limited to the PPARγ2 protein because similar effects were observed when analogous mutations were generated in the PPARγ1 isoform as well as in the related PPARα and PPARβ/δ proteins.

### Corepressor Binding and Release of PPARγ2 R425C Is Impaired

Mutations in the thyroid hormone receptor β (TRβ) are found in patients with resistance to thyroid hormone (RTH) (40). One RTH-associated mutation changes an arginine at position 383 into a histidine (R383H), resulting in impaired release of the corepressor SMRT (41). Because R383 in TRβ is analogous to R425 in PPARγ2 (Fig. 3A), the effect of the R425C mutation in PPARγ2 on binding and release of SMRT was investigated. For this, bacterially expressed and purified glutathione-S-transferase (GST) or GST-SMRT fusion proteins were incubated with *in vitro*-translated [$^{35}$S]methionine-labeled PPARγ2 proteins (wild type or R425C) in the absence or presence of rosiglitazone. As shown in Fig. 3B, wild-type PPARγ2 interacted with SMRT in the absence of ligand, and this interaction was reduced upon addition of rosiglitazone (Fig. 3B). The PPARγ2 R425C mutant interacted with SMRT less efficiently, both in the absence and presence of ligand and did not show an obvious impairment of SMRT release in response to ligand (Fig. 3B).

To substantiate these *in vitro* results in living cells, we performed mammalian two-hybrid assays. For this, an expression vector consisting of the interaction domain 1 (ID1) of SMRT fused to the DBD of Gal4 (Gal4DBD) were used, together with an expression vector encoding a fusion protein of PPARγLBD with the activation domain of viral protein 16 of herpes simplex virus (VP16). In the absence of ligand, wild-type PPARγLBD clearly interacted with the SMRT-ID1, as demonstrated by the activation of the 5xGal4-TK-Luc reporter (Fig. 3C). Upon addition of rosiglitazone, this interaction decreased in a dose-dependent manner. In contrast, PPARγLBD R425C showed limited interaction with SMRT-ID1, either in the absence or presence of ligand. In contrast, the FPLD3-associated

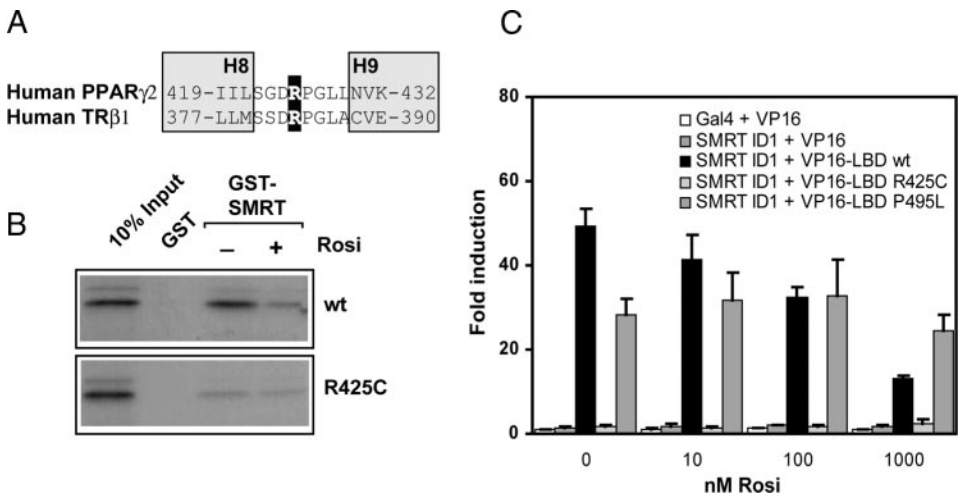


**Fig. 3.** The PPARγ2 R425C Mutation Affects Corepressor Binding But Not Release

A, Alignment of the amino acid sequence surrounding R425 in human PPARγ2 and human TRβ1 (AAI06930). B, GST fusion proteins coupled to Sepharose beads were incubated with *in vitro*-translated [$^{35}$S]-labeled PPARγ2 proteins [wild type (wt) or mutant] in the absence or presence of rosiglitazone (Rosi; 1 μM). After extensive washing, samples were boiled and separated on SDS-polyacrylamide gels. Gels were fixed and dried and the labeled proteins were detected by fluorography. The input lanes represent 10% of the total lysate used in each reaction. C, U2OS cells were transfected with Gal4DBD or Gal4DBD-SMRT ID1 (50 ng), VP16 or VP16-PPARγLBD (wt or mutant; 50 ng), 5xGal4-TK-Luc reporter (500 ng) and incubated with different concentrations of rosiglitazone as indicated. Activation of the luciferase reporter, in the absence or presence of rosiglitazone, is expressed as fold induction over that with Gal4DBD+VP16 in the absence of ligand, after normalization for *Renilla* luciferase activity. Results are averages of at least three independent experiments assayed in duplicate ± SEM.

P495L mutant of PPARγ2, which was previously shown to exhibit impaired corepressor release (37), showed a comparable level of transcriptional activity at all concentrations of rosiglitazone. The negative controls, in which VP16 protein was coexpressed with either Gal4DBD or Gal4DBD-SMRT-ID1, displayed negligible luciferase activity.

Thus, our data indicate that the R425C mutation in PPARγ2 does not impair corepressor release, but rather reduces the affinity for the corepressor. We conclude, therefore, that in contrast to the natural R383H mutant of TRβ, the reduction in PPARγ-mediated transcription caused by the R425C mutation is unlikely to be caused by impaired corepressor release.

### The PPARγ2 R425C Mutation Results in Reduced Heterodimerization with RXRα

The crystal structure of PPARγ-LBD reveals 13 α-helices and a small four-stranded β-sheet (16, 17). The arginine at position 425 lies within a highly conserved sequence that is located in a loop between helix 8 and 9, and some of the residues surrounding arginine 425 (G423, D424, and P426) are involved in heterodimerization with RXRα. This prompted us to investigate whether the PPARγ R425C mutation affected dimerization with RXRα. First, we studied the effect of this mutation and mutations of the other highly conserved loop residues on *in vitro* heterodimerization by performing GST-pull down assays. For this, *in vitro*-translated [$^{35}$S]methionine-labeled PPARγ2 proteins (wild type or mutants) were incubated with bacterially expressed and purified GST-RXRα. Whereas wild-type PPARγ2 efficiently interacted with RXRα, the R425C mutant protein displayed reduced binding (Fig. 4A). Mutation of arginine 425 into alanine (R425A) or lysine (R425K) also decreased the PPARγ2-RXRα interaction. PPARγ2 D424A showed a slightly reduced binding compared with wild-type PPARγ2, whereas mutation of glycine 423 or proline 426 into alanine (G423A and P426A, respectively) did not have an appreciable effect on *in vitro* dimerization with RXRα. As a control, a PPARγ2 mutant was generated (L464R), analogous to the homodimerization-defective mouse ER mutant (L511R) (42). This L464R mutant completely failed to dimerize with RXRα in these *in vitro* assays (Fig. 4A).

Next, the effects of the mutants described above on the transcriptional activity of PPARγ2 were studied. Like the R425C mutant (Fig. 1), the R425A and R425K mutants displayed strongly reduced ligand-dependent activation of a 3xPPRE-tk-Luc reporter in U2OS cells (Fig. 4B). The D424A mutant showed slightly reduced transcriptional activity, whereas the activity of the G423A and P426A mutants was similar to wild-type PPARγ2. Transcriptional activity of the heterodimerization-defective mutant L464R was completely abolished. The expression of all PPARγ proteins was confirmed by Western blot analysis (Fig. 4B, *lower panel*). In general, the observed differences in transcriptional levels between the PPARγ2 mutants reflected the differential effects on heterodimerization of these mutants (Fig. 4A), confirming that heterodimerization is a prerequisite for the transcriptional activity of the

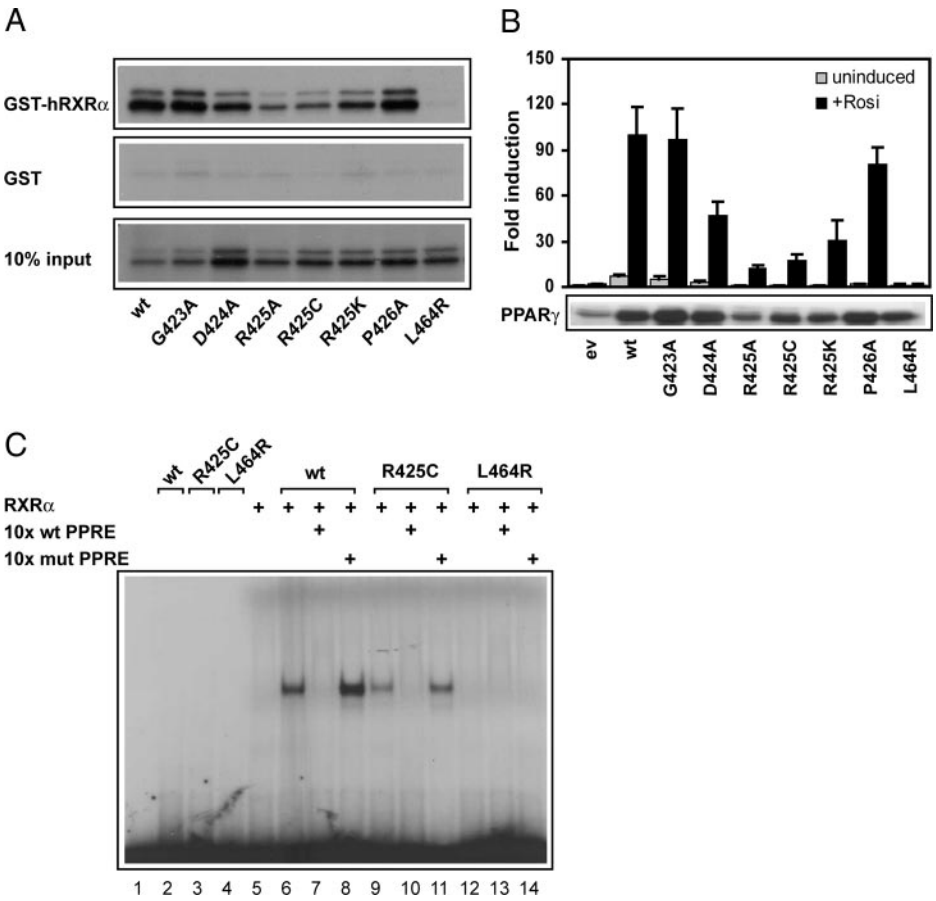


**Fig. 4.** Heterodimerization of PPARγ2 R425C with RXRα and Subsequent DNA Binding Is Impaired

A, Bacterially expressed and purified GST or GST-RXRα proteins were incubated with *in vitro*-translated [$^{35}$S]methionine-labeled PPARγ2 proteins [wild type (wt) or mutant]. Bound proteins were visualized as described in Fig. 3B. B, U2OS cells were transfected with various PPARγ2 mutants. Experiments were performed and data are presented as described in Fig. 1A. Expression of the different PPARγ2 proteins was confirmed by Western blot analysis using an antibody directed against PPARγ. C, *In vitro*-translated RXRα or PPARγ2 (wt or mutant) proteins were incubated with [$^{32}$P]-labeled probe in absence or presence of 10× unlabeled probe (wt or mutant) as indicated. Protein-DNA complexes were separated from unbound DNA on nondenaturing SDS-polyacrylamide gels and visualized by autoradiography of dried gels. ev, Empty vector; wt, wild type.

PPARγ2 protein. In addition, mutation of the positively charged arginine at position 425 into a cysteine (R425C), into the uncharged residue alanine (R425A) or into a lysine residue (R425K), which is also positively charged, all affected the *in vitro* RXRα heterodimerization capacity as well as the transcriptional activity of PPARγ2. These findings point to the specific requirement of the arginine residue at position 425 for optimal function of PPARγ2 as a transcription factor.

Because PPARγ can only bind to PPRE sequences in the DNA upon heterodimerization with RXRα, we investigated the effect of the R425C mutant on DNA binding. EMSAs were performed in which *in vitro*-translated RXRα and PPARγ2 proteins (either wild type or mutant) were incubated with a [$^{32}$P]-labeled PPRE sequence. A specific PPARγ2-RXRα heterodimeric complex was formed on the PPRE because formation of this protein-DNA complex could be diminished by addition of an excess of unlabeled wild-type PPRE, but not by an excess of mutant PPRE (Fig. 4C). The R425C mutant protein also displayed specific DNA binding in the presence of RXRα, albeit 2.3-fold less than wild type, as determined by densitometric analysis. A similar difference in binding capacity was observed with increasing amounts of PPARγ2 protein (wild type or R425C) (see supplemental Figure S1, which is published as supplemental data on The Endocrine Society's Journals Online web site at http://mend.endojournals.org). Specific antibodies against PPARγ and RXRα supershifted both the wild-type and mutant protein-DNA complexes, confirming the heterodimeric composition of both complexes (see supplemental data Figure S2). The dimerization-defective L464R mutant failed to bind the PPRE in the presence of RXRα (Fig. 4C). Taken together, these results indicate that heterodimerization with RXRα and subsequent DNA binding of PPARγ2 is significantly, but not completely impaired by the R425C mutation.

### Ligand Binding and Subsequent Coactivator Binding of PPARγ2 R425C Is Reduced

Because heterodimerization with RXRα and subsequent DNA binding of PPARγ2 R425C is not completely impaired, this suggests that additional molecular defects contribute to the impaired function of this FPLD3-associated mutant. To investigate this, we performed reporter assays in which PPARγ driven transcription is independent of heterodimerization with RXRα. For this, the mutations described above were introduced into a chimeric Gal4DBD-PPARγ LBD receptor and expressed together with a Gal4 reporter gene in U2OS cells. Both the wild-type Gal4-PPARγLBD receptor and the dimerization defective L464R mutant stimulated transcription from the reporter up to 350-fold in the presence of rosiglitazone, showing that transcriptional activation is indeed independent of heterodimerization with RXRα in this assay (Fig. 5A). In contrast, the activity of the R425C mutant, as well as the R425A and R425K mutants, was strongly reduced. The G423A, D4242A and P426A mutants displayed levels of transcription similar to wild-type PPARγ. As a control, Western blot analysis was performed and showed comparable amounts of GAL4DBD fusion proteins (Fig. 5A, *lower panel*). These results indicate that the transcriptional defect in the PPARγ2 R425C protein is not only due to reduced heterodimerization with RXRα.

To identify additional defects in the R425C protein, we first performed ligand binding assays. For this, bacterially expressed and purified GST-PPARγ2 fusion proteins (wild type or R425C) were incubated with either 10 nM or 100 nM of [$^3$H]-labeled rosiglitazone. Whereas wild-type PPARγ2 protein displayed specific binding of rosiglitazone, the mutant protein showed reduced binding capacity for the ligand at both concentrations tested (Fig. 5B). The amounts of the bacterially produced receptors were similar (Fig. 5B, *inset*), indicating that the lower binding capacity for rosiglitazone displayed by the mutant protein was not caused by differences in protein levels. Because a

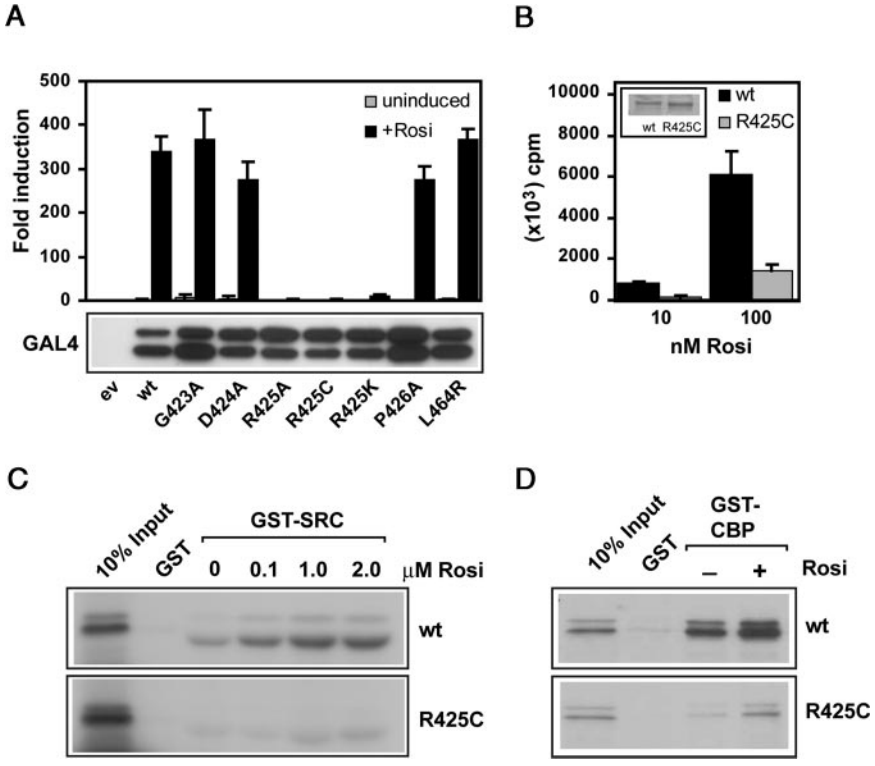


**Fig. 5.** Ligand Binding and Subsequent Coactivator Binding of PPARγ2 R425C Is Reduced

A, U2OS cells were transfected with 5xGal4-AdMLTATA-Luc reporter (1 μg), empty vector (ev) or Gal4DBD-PPARγLBD expression vectors [wild type (wt) or mutant; 200 ng] and incubated with or without rosiglitazone (Rosi; 1 μM) as indicated. Data are presented as described in Fig. 1A. Comparable amounts of the different GAL4 DBD fusion proteins were detected by Western blot analysis using a GAL4 antibody. B, GST-PPARγ2 (wt or mutant) was incubated with different concentrations of [$^3$H]-rosiglitazone. Bound ligand was measured by a γ-counter. Data are indicated as mean of three separate experiments performed in duplicate. *Inset*, Bacterially expressed and purified PPARγ2 proteins (wt or mutant) were subjected to SDS-PAGE and visualized by Coomassie brilliant blue staining. C, *In vitro*-translated [$^{35}$S]-labeled PPARγ2 proteins (wt or mutant) were incubated with bacterially expressed and purified GST or GST-SRC1 in the absence or presence of increasing concentrations of rosiglitazone (0.1, 1, or 2 μM). Bound proteins were visualized by fluorography of dried gels. D, *In vitro*-translated [$^{35}$S]-labeled PPARγ2 proteins (wt or mutant) were incubated with bacterially expressed and purified GST or GST-CBP in the absence or presence of rosiglitazone (1 μM). Bound proteins were visualized by fluorography of dried gels.

coactivator binding surface is generated in the LBD of PPARγ upon ligand binding, we next examined whether the reduced affinity for rosiglitazone displayed by the R425C protein also affected interaction with coactivators. For this, bacterially expressed and purified GST-fusion proteins of the coactivators CBP and SRC1 were incubated together with *in vitro*-translated [$^{35}$S]methionine-labeled PPARγ2 wild-type or PPARγ2 R425C proteins in the absence or presence of rosiglitazone. As observed before (43–45), wild-type PPARγ2 bound to SRC1 in the presence of rosiglitazone in a dose-dependent manner (Fig. 5C), whereas the interaction between PPARγ2 and CBP was less dependent on the presence of ligand (Fig. 5D). Although PPARγ2 R425C also displayed specific binding to SRC1 and CBP under these conditions, these protein-protein interactions were significantly weaker compared with wild-type PPARγ2.

In summary, these experiments indicate that, in addition to impaired heterodimerization (Fig. 4), the R425C mutation also abrogates ligand binding compared with the wild-type protein and as a consequence diminishes ligand-dependent interaction with transcriptional coactivators.

### Transrepression of NF-κB by PPARγ R425C Remains Largely Intact and Is Independent of Heterodimerization with RXRα

To examine the effect of the R425C mutation on PPARγ-mediated repression of NF-κB activity, we performed reporter assays in which U2OS cells were transfected with expression vectors encoding wild-type PPARγ2 or mutant PPARγ (R425C or L464R) or an empty vector together with a 2κB-luciferase reporter. Upon addition of TNFα, this reporter was activated up to 10-fold and cotransfection of increasing amounts of either wild-type PPARγ2 or R425C both reduced this activation in a dose-dependent manner. Addition of rosiglitazone enhanced this inhibitory effect to some extent (Fig. 6A). Because the R425C mutant displayed reduced dimerization with RXRα (Fig. 4), these results suggest that monomeric forms of the receptor may be sufficient for transrepression of NF-κB activity, as was also shown for other nuclear receptors (46). To investigate this, we employed the PPARγ2 L464R mutant, which displays a complete loss of dimerization activity (Fig. 4). A dose-dependent decrease in reporter activation by TNFα was observed upon addition of increasing amounts of L464R mutant, corroborating the hypothesis that PPARγ-mediated transrepression of NF-κB is independent of heterodimerization with RXRα.

In addition, because transcriptional interference between PPARγ and NF-κB occurs through the RelA (p65) subunit of NF-κB (47), we assessed this protein-protein interaction by incubating bacterially expressed GST-RelA fusion proteins with *in vitro*-translated PPARγ2 proteins (either wild type, R425C, or L464R). As shown in Fig. 6B, all three PPARγ2 proteins were able to bind to GST-RelA and this interaction was largely rosiglitazone independent.

In summary, although the FPLD3-associated R425C mutation results in reduced transcriptional activity of PPARγ (Fig. 1), PPARγ-mediated transrepression of NF-κB activity remains largely intact, especially in the presence of ligand. Furthermore, our data suggest that

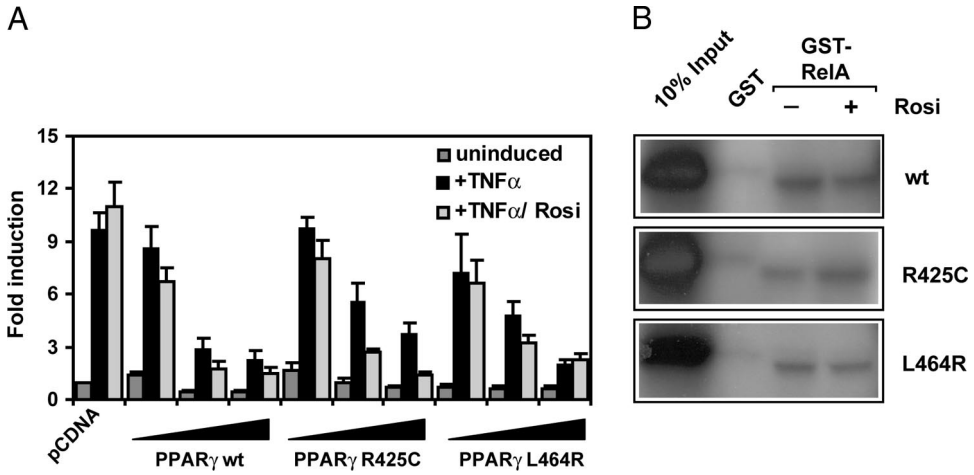


**Fig. 6.** The FPLD3-Associated PPARγ R425C Mutation Is Able to Transrepress NF-κB Activity

A, U2OS were transfected with empty vector (10 ng), wild-type (wt) PPARγ2, PPARγ2 R425C, and PPARγ2 L464R, respectively (10, 50, or 100 ng) and 2κB-luciferase reporter (300 ng). Activation of the luciferase reporter in the absence or presence TNFα (250 U) or TNFα in combination with rosiglitazone (Rosi; 1 μM), respectively, is expressed as fold induction over that of empty vector in the absence of TNFα and rosiglitazone, after normalization for *Renilla* luciferase activity. Results are averages of three independent experiments performed in duplicate ± SEM. B, *In vitro*-translated [$^{35}$S]-labeled PPARγ2 proteins (wt, R425C or L464R) were incubated with bacterially expressed and purified GST or GST-RelA in the absence or presence of rosiglitazone (1 μM). Bound proteins were visualized by fluorography of dried gels.

the PPARγ-mediated transrepression is largely independent of heterodimerization with RXR.

### Molecular Dynamics Simulation Predicts an Alternative Salt Bridge in PPARγ2 R425C

Because the arginine residue on position 425 in PPARγ2 is involved in the formation of an internal salt bridge (16), the effects of substituting this amino acid by cysteine was examined using several 5-nsec molecular dynamics simulations of wild-type protein and R425A and R425C mutants starting from various crystal structures of the LBD domain of PPARγ (see *Materials and Methods*). Positional root mean square deviation from the starting structures as well as the various energy terms reached equilibrium in a few nsec for all the simulations (see supplemental data Figures S3 and S4). When analyzing the trajectories resulting from the different simulations, there was a clear and consistent difference between wild-type PPARγ2 and PPARγ2 R425C with respect to salt bridges that are present. In the wild-type protein, R425 (located in the loop between helix 8 and 9) forms a salt bridge with E352 (in helix 4/5), and R471 (in helix 10) forms a salt bridge with D424 (Fig. 7A, *left panel*). In the R425C mutant, however, the salt bridge between R425 and E352 obviously cannot be formed, and this resulted, unexpectedly, in a switch from the R471-D424 salt bridge to a salt bridge between R471 and E352 (Fig. 7A, *right panel*, and supplemental data Figure S5). A similar change was observed when R425 was mutated into alanine (data not shown). We also compared various structural parameters (root mean square deviations, angles between helices, solvent accessibility of surface residues). Although in some simulations helix 10 seemed to be deformed in the R425C mutant, we could not find consistent differences between wild-type and mutant simulations. The difference in salt bridge pattern was consistently found between on the one hand the three wild-type simulations and on the other hand four mutant simulations

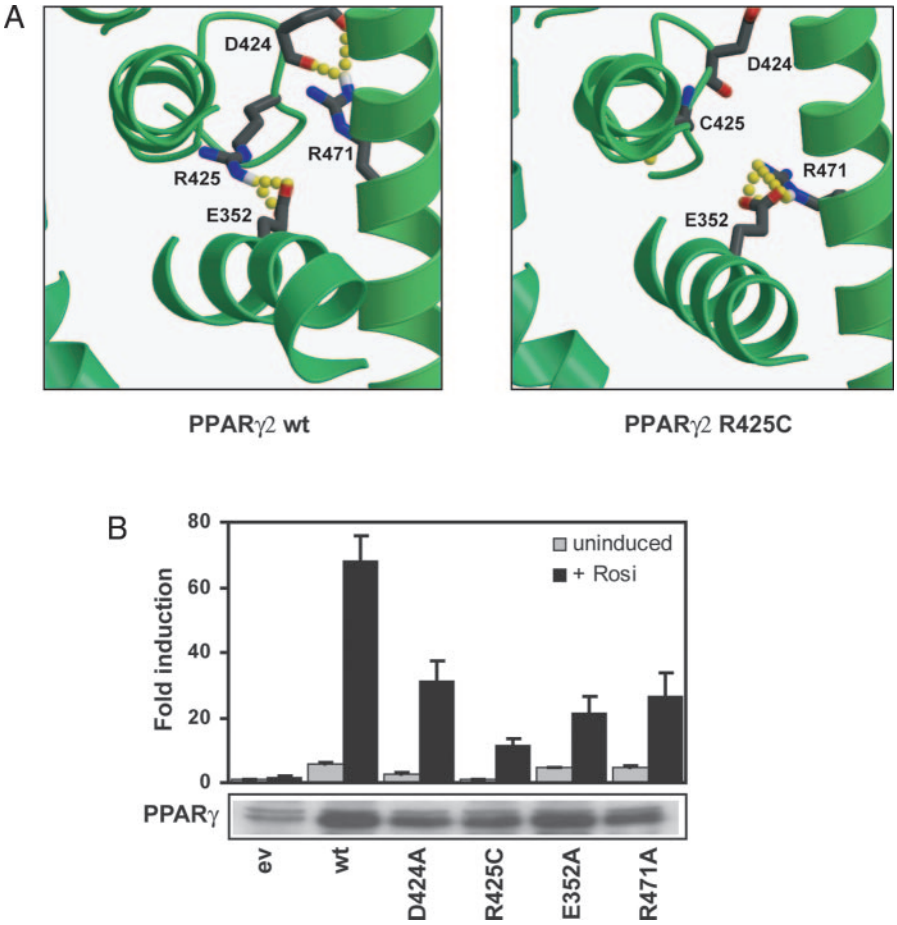


**Fig. 7.** An Internal Salt Bridge in PPARγ2 Is Disturbed by the Substitution of Arginine 425 with Cysteine

A, Snapshots from molecular dynamics simulations for wild-type (wt; *left panel*) and R425C (*right panel*) mutant PPARγ. A close-up view of the salt bridges discussed in the text is provided, with residues involved represented in ball-and-stick. B, U2OS cells were transfected with vectors expressing various mutants of PPARγ2. Experiments were performed and data are presented as described in Fig. 1A. Expression of the different PPARγ2 proteins was confirmed by Western blot analysis using an antibody directed against PPARγ. Rosi, Rosiglitazone.

(both R425A and R425C). The fact that the same rearrangement is observed in independent simulations starting from various crystal structures, make the observed structural difference between wild-type and mutant protein highly significant.

To test the importance of those salt bridges for transcriptional activity, we mutated the individual residues involved in the salt bridge formation to alanine residues and performed reporter assays in U2OS cells. Like R425C, the salt bridge mutants D424A, E352A and R471A all displayed reduced transcriptional activity compared with wild-type PPARγ2 (Fig. 7B). Western blot analysis was performed as a control and showed comparable expression levels for all PPARγ proteins (Fig. 7B, *lower panel*). These findings suggest that the internal salt bridges between R425 and E352 and between D424 and R471 play an important role in PPARγ2-mediated transcription by maintaining the structural integrity of the LBD of this receptor.

### PPARγ2 R425C and PPARγ1 R397C Do Not Display Dominant-Negative Behavior

All of the FPLD3-associated PPARγ mutations are heterozygous and some of the resulting PPARγ mutant proteins have been shown to inhibit their wild-type counterpart in a dominant-negative manner (29, 37). We therefore examined whether the R425C mutant of PPARγ2 and the same mutant in the context of the PPARγ1 protein (R397C) would inhibit the activity of the respective wild-type receptors. For this, reporter assays were performed, using a 1:1 ratio between wild-type and mutant receptors and different concentrations of ligand. As shown in Fig. 8A, PPARγ1 R397C failed to display dominant-negative behavior independent of ligand concentration, whereas the FPLD3-associated PPARγ1 P467L inhibited wild-type PPARγ1 at low concentrations of ligand, as reported earlier (37). In addition, the artificial PPARγ1 L468A/E471A mutant displayed a strong dominant-negative activity against its wild-type protein independent of ligand concentration, as shown earlier (48).

When tested in the context of the PPARγ2 protein, the R-to-C mutant also lacked dominant-negative activity, whereas PPARγ2 L496A/E499A was able to inhibit wild-type PPARγ2 at all concentrations of rosiglitazone (Fig. 8B). Interestingly, whereas PPARγ1 P467L displayed a dominant-negative effect over its wild-type counterpart (Fig. 8A), the same mutant in the context of PPARγ2 (P495L) was not able to inhibit wild-type receptor in a dominant-negative manner (Fig. 8B). In addition, the PPARγ1 P467L mutant was dominant-negative over wild-type PPARγ2, but PPARγ2 P495L did not display dominant-negative activity over wild-type PPARγ1 (data not shown). Similar results were obtained in 293T cells, indicating that the observed effects were not restricted to U2OS cells (data not shown).

In summary, these data show that unlike the artificial PPARγ double mutant, the FPLD3-associated PPARγ R-to-C mutant does not exert dominant-negative activity over the wild-type receptor, whereas dominant-negative activity of the FPLD3-associated PPARγ P-to-L mutant appears to be limited to the PPARγ1 isoform under our experimental conditions.

### The R425C Mutation Reduces the Ability of PPARγ2 to Induce Adipocyte Differentiation

Having established by *in vitro* and cell-based assays that PPARγ function is affected on multiple levels we investigated the effect of this mutation *in vivo* on adipocyte differentiation. NIH-3T3 fibroblasts were transduced with virus obtained from cells transfected with

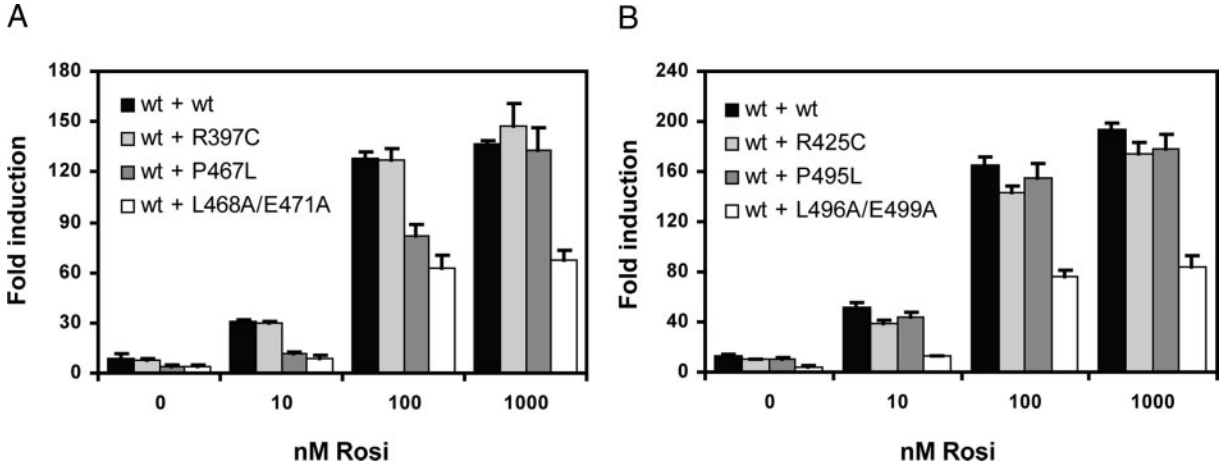


**Fig. 8.** FPLD3-Associated R-to-C Mutants Fail to Display Dominant-Negative Activity toward Wild-Type PPARγ Isoforms

A, U2OS cells were transfected with equal amounts of wild-type (wt) and mutant PPARγ1 (both 100 ng), 3xPPRE-tk-Luc reporter (500 ng) and incubated with different concentrations of rosiglitazone (Rosi), as indicated. B, U2OS were transfected as in panel A, but with PPARγ2 expression vectors. Results are averages of at least three independent experiments assayed in duplicate ± SEM.

the parental retroviral pMSCV vector, pMSCV-PPARγ2 or pMSCV-PPARγ2 R425C and stable cell lines were selected. Approximately 20% of the NIH-PPARγ2 cells differentiated into adipocytes, as assessed by staining of triglycerides with Oil-red-O (Fig. 9A). Virtually no adipocyte differentiation could be detected in NIH-vector or NIH-PPARγ2 R425C fibroblasts under our experimental conditions. To independently confirm adipocyte differentiation, the mRNA expression of three PPARγ target genes, fatty acid binding protein 4 (*Fabp4*), adipose aquaporin (*Aqp7*) and glycerol kinase (*Gyk*), was determined on the same cell lines by quantitative RT-PCR assays. Whereas a 34-fold increase in *Fabp4* mRNA expression was observed for NIH-PPARγ2 cells, mRNA expression of this gene in NIH-PPARγ2 R425C cells was similar to NIH-vector cells (Fig. 9B). The PPARγ2 R425C protein also failed to induce mRNA expression of *Aqp7* and *Gyk*, both of which were significantly up-regulated by the wild-type receptor (Fig. 9B). As shown by Western blot analysis, the PPARγ protein expression levels for wild-type and R425C proteins were similar (Fig. 9C).

These findings show that the R425C mutation not only compromises the ability of the PPARγ2 protein to activate transiently transfected reporter genes (Fig. 1) but also reduces its potential to activate endogenous target genes (*Fabp4*, *Aqp7*, *Gyk*) and promote adipogenesis (Fig. 9).

## DISCUSSION

The nuclear receptor PPARγ plays a key role in the regulation of glucose and lipid metabolism in adipocytes by regulating their differentiation, maintenance, and function (9, 10). Compelling genetic evidence for this view comes from human FPLD3 patients, harboring heterozygous mutations in the *PPARG* gene, because they are characterized by aberrant fat distribution and metabolic disturbances, including insulin resistance and dyslipidemia (6, 7). In this report, we demonstrate that the FPLD3-associated PPARγ2 R425C mutant displays multiple molecular defects. These defects probably do not involve impaired corepressor release, but comprise a combination of reduced heterodimerization with RXRα, lower ligand binding affinity and subsequent reduced binding of coactivators, resulting in reduced transcriptional activity and eventually in an impaired ability of the R425C mutant to induce adipocyte differentiation. Interestingly, like the dimerization-defective L464R mutant, the R425C mutant could still transrepress TNFα-in-

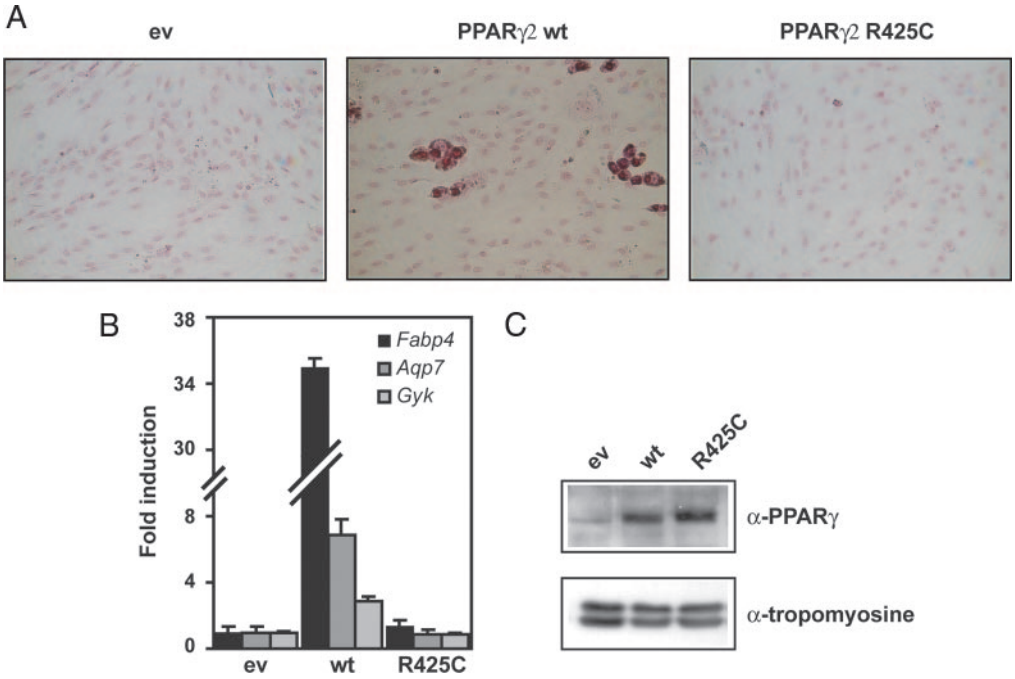


**Fig. 9.** Reduced Potential of the PPARγ2 R425C to Induce Adipocyte Differentiation

A, NIH-3T3 fibroblasts were transduced with retrovirus obtained from cells transfected with pMSCV (empty vector; ev), pMSCV-PPARγ2, or pMSCV-PPARγ2 R425C. After a week of incubation with differentiation medium, triglycerides were stained with Oil-Red-O and cell nuclei with crystal violet. Pictures are representative for three independent experiments. B, mRNA expression of the Fabp4, Aqp7, and Gyk genes in NIH-3T3 cell lines described in panel A after differentiation. Expression levels are indicated as fold induction over that with NIH-ev cells, after normalization for the housekeeping gene Hprt1. Results are averages of at least three independent experiments assayed in duplicate ± SD. C, Western blot analysis of lysates of the NIH-3T3 cell lines described in panel A with antibodies against PPARγ and tropomyosine (internal control).

duced NF-κB activity. These results are reminiscent of the transrepression of NF-κB activity by monomeric forms of other nuclear receptors, like the glucocorticoid receptor (46), and indicate that activation and transrepression critically depend on different regions of the receptor (49). Recently, a structure based sequence alignment revealed two sets of differentially conserved residues that divided the entire nuclear receptor superfamily in two classes related to their oligomeric behavior (35). Nuclear receptors that form homodimers belong to class I, whereas nuclear receptors that form heterodimers with RXRα, like PPARγ, belong to class II. A differentially conserved arginine (R425 in PPARγ2) defines the signature of these class II receptors and is involved in the formation of a salt bridge with a negatively charged residue in H4/H5 (E352 in PPARγ2) (16, 17). Moreover, the crystal structure of PPARγ LBD revealed an additional internal salt bridge between two different conserved class II residues, D424 (L8/9) and R471 (H10). Our molecular dynamics simulations predicted that substitution of PPARγ2 R425 with a cysteine residue would disrupt both internal salt bridges leading to the formation of an alternative salt bridge between R471 and E352. The conserved salt bridge residues are structurally important in defining the conformation of the LBD of PPARγ2: both D424 and R471 are involved in dimerization with RXRα (16), whereas R425 and E352 form hydrogen bonds with Y505 at the C terminus of helix 12 leading to the stabilization of H12, which is important for cofactor binding (39). In addition, destabilization of H12 could in turn affect heterodimerization because an interdimer salt bridge is formed between Y505 (H12) of PPARγ2 and K431 of RXRα (16). Finally, crystallographic studies on PPARα, together with a corepressor peptide, indicate that the two hydrophobic residues immediately preceding E352 in PPARγ2 are probably part of the corepressor interaction surface (50). Therefore, conformational changes resulting from the simultaneous disruption of both internal salt bridges through the R425C mutation provide a likely explanation for the impaired interactions with cofactors and RXRα, as well as the reduction in ligand binding, despite the fact that R425 is not in the direct vicinity of the ligand binding pocket. The partial restoration of PPARγ2 R425C activity by the tyrosine-based agonist GW1929 might be explained by the benzophenone group in this type of ligand, which is not present in TZDs. This group can make additional hydrophobic interactions with residues in H3, H7, and H10 (16), which could contribute to the active conformation of the LBD structure and thereby partially restore the activity of PPARγ2 R425C, as was observed specifically with this ligand.

Studies on four other mammalian class II nuclear receptors, vitamin D receptor (VDR), TRβ, RXRα and retinoic acid receptor α (RARα), have pointed to the importance of the conserved salt bridge residues for their function. In keeping with our results on the E352A mutation in PPARγ2, the analogous mutant in VDR (E269A) displayed reduced ligand binding and transcriptional activity (51). Unlike the PPARγ2 R425C mutant, however, mutation of the analogous residue in TRβ, as exemplified by the RTH-associated R383H mutant, did not affect activation of target genes, but resulted in impaired corepressor release (41). Furthermore, the R339A mutation reduced the transcriptional activity of RARα, but heterodimerization was unaffected (35), which is in contrast to the analogous PPARγ2 mutant (R425A). Finally, the D384A mutant of RXRα (D424A in PPARγ2) displayed reduced ability to homodimerize, but heterodimerization with RARα was unaffected (52). These findings therefore clearly underscore the important role of the internal salt bridges in maintaining the structural integrity of the LBDs of class II receptors, but also show that the molecular defect(s) caused by their disruption can differ between individual nuclear receptors.

Although the PPARγ2 R425C mutant displays some similarities with other FPLD3-associated PPARγ mutants, the molecular defects are clearly not identical. Based on functional characterizations in combination with studies on dominant-negative activity of these different PPARγ mutants, PPARG mutations can be divided in at least three different subgroups (29–34, 37). The first group comprises the missense DNA binding mutants and LBD truncation mutants (C142R, C159Y, C190W, FS343X, R385X). These mutants have no DNA binding capacity but are still able to recruit coactivators and can therefore compete for common cofactors (squelching), which can explain their dominant-negative activity. The second group consists of missense mutations located in the LBD (V318M, P495L), which inhibit PPARγ activity through an alternative mechanism. These mutants are transcriptionally inactive due to impaired ligand and coactivator recruitment but are able to compete for DNA binding with wild-type PPARγ. As a consequence the activation of PPARγ target genes is reduced, which could explain the dominant-negative activity of these mutants. The third group, represented by the PPARγ R425C mutant, displays both impaired heterodimerization with RXRα and subsequent DNA binding, as well as impaired ligand and cofactor binding, the combination of which could account for the absence of dominant-negative activity. In line with this, addition of an artificial mutation in TRβ, which attenuated heterodimerization with RXRα and subsequent DNA binding, abrogated the dominant-negative activity of three different natural LBD mutants (53, 54). This suggests that the combination of either intact DNA binding, together with impaired cofactor binding, or intact cofactor binding in combination with impaired DNA binding is a prerequisite for dominant-negative activity of TRβ and PPARγ mutants. Like the R425C mutant analyzed here, the FPLD3-associated PPARγ2 F388L mutant (30) and the recently published nonsense mutation, which truncates PPARγ2 after residue 355 (Y355X) (33), also lack dominant-negative behavior. Together with the FPLD3-associated PPARγ4 promoter (-14A>G) muta-

tion (55), which only reduces the expression of the PPARγ protein, these findings indicate that in some FPLD3 patients *PPARG* mutations act through a haploinsufficiency mechanism rather than dominant-negative activity of the affected gene product.

When the FPLD3-associated PPARγ P-to-L mutant was tested in the context of the PPARγ1 protein (P467L), this protein inhibited wild-type PPARγ1 and -γ2 in a dominant-negative fashion at low concentrations of rosiglitazone, as described earlier (37). Interestingly, the same amino acid substitution in the context of the PPARγ2 protein (P495L) resulted in a protein that lacked this capacity, indicating that at least under our experimental conditions the dominant-negative activity of the PPARγ P-to-L mutant is isoform specific. These findings suggest that the effect of dominant-negative PPARγ mutants might be more pronounced in tissues with a high PPARγ1/-γ2 ratio, but it is currently unknown whether this ratio differs between body fat depots. An important challenge for the future will be to establish how heterozygous *PPARG* mutations can lead to depot-specific effects on adipose tissue, as exemplified by the characteristic aberrant fat distribution in patients suffering from FPLD3 and mice expressing PPARγ mutants (56, 57).

## MATERIALS AND METHODS

### Materials

Rosiglitazone was purchased from Alexis (Lausen, Switzerland). Pioglitazone, ciglitazone, troglitazone, and 15-deoxy-$\Delta^{12,14}$-$PGJ_2$ were from Cayman Chemical Co. (Ann Arbor, MI). GW1929 and TNFα were from Sigma-Aldrich (St. Louis, MO). [$^3$H]-rosiglitazone was purchased from American Radiolabeled Chemicals, Inc. (St. Louis, MO). Fugene 6 transfection reagent was from Roche Applied Biosciences (Indianapolis, IN). Anti-PPARγ (sc-7273), anti-RXRα (sc-553), and anti-Gal4 (sc-510) antibodies were from Santa Cruz Biotechnologies (Santa Cruz, CA). Anti-tropomyosin antibody (T2780) was purchased from Sigma-Aldrich and Roche Applied Biosciences, respectively. Antirabbit-horseradish peroxidase (111035144) and antimouse-horseradish peroxidase (115035146) were from Jackson ImmunoResearch Laboratories Inc. (West Grove, PA). Oil-Red-O was purchased from Sigma-Aldrich (O-0625). Crystal violet was from Chroma-Gesellschaft Schmid & Co. (Köngen, Germany).

### Plasmids

All recombinant DNA work was performed according to standard procedures (58). The pCDNA3-PPARγ1, pCDNA3-PPARγ2 and pCDNA3-PPARβ/δ constructs were kind gifts from Dr. V. K. K. Chatterjee (Department of Medicine, University of Cambridge, Cambridge, UK) (48). pCDNA3.1-PPARα expression plasmid was a kind gift from Dr. S. Ali (Imperial College London, London, UK). The reporter containing the human aquaporin promoter (−681/+11) was a kind gift from Dr. N. Maeda (Osaka University, Osaka, Japan) (38). The reporter plasmid 2κB-luciferase was a kind gift from Dr. E. Burstein (University of Michigan, Ann Arbor, MI) (59). The retroviral pMSCV-vector (CLONTECH, Palo Alto, CA) containing wild-type murine PPARγ2 was a kind gift from Dr. B. M. Spiegelman (Dana-Farber Cancer Institute, Harvard Medical School, Boston, MA) and Dr. R. G. Roeder (Rockefeller University, New York, NY) (60). The bacterial expression vector for GST-SMRT (61) and the 3xPPRE-tk-Luc reporter (23) were kind gifts from Dr. R. M. Evans (Howard Hughes Medical Institute and Gene Expression Laboratory, Salk Institute, La Jolla, CA). The bacterial expression vector for GST-SRC1 (amino acids 570–780) (62), GST-RelA (63) and the 5xGal4-AdMLTATA-Luc (64), 5xGal4-TK-Luc (64), and 3xPPRE-tk-Luc (23) reporters have been described earlier.

The pCDNA-Gal4DBD-PPARγ LBD (amino acids 173–475) expression construct was generated by cloning a *Bam*H1/*Xba*1 fragment from pSG424-PPARγLBD (gift from Dr. V. K. K. Chatterjee (48) into the respective sites of pCDNA3-Gal4DBD (64). The expression vector containing the complete coding region of human RXRα was a kind gift from Dr. J. D. Baxter (65). pCDNA3.1-RXRα was generated by PCR amplification of RXRα from this vector using primers containing *Xba*I and *Hin*dIII-sites and cloned into the respective sites of pCDNA3.1(-). PGEX2TK-GST-CBP was generated by cloning the *Bam*HI/*Eco*RI fragment (amino acids 1–452) from pCDNA3.1-CBP (64) into the pGEX2TK vector. To generate a pCDNA3-Gal4DBD-SMRT-ID1 construct, the SMRT-ID1 fragment (amino acids 2302–2352) was amplified from the GST-SMRT construct (61) by PCR using primers containing *Bam*H1and *Xba*I-sites, respectively, and cloned into the pCDNA3-Gal4DBD construct. PCDNA3-VP16 was constructed by amplification of the VP16 from a psG5-VP16 expression construct (66) by PCR using a forward primer containing a *Hin*dIII-site and a reverse primer containing a stopcodon and *Bam*H1-site. The VP16 cDNA was inserted in the corresponding sites of pCDNA3. PCDNA3-VP16-PPARγLBD was generated by PCR amplification of VP16 activation domain using primers containing *Hin*dIII and *Bam*H1-sites, respectively, and insertion into the respective sites of pCDNA-Gal4DBD-PPARγLBD, after removal of the Gal4DBD sequence. All mutations were generated by QuikChange mutagenesis (Stratagene, La Jolla, CA) and verified by sequencing.

### Cell Culture, Transient Transfections, and Reporter Assays

The human osteosarcoma cell line U2OS and the human embryonic kidney 293T cell line (HEK293T) were maintained in DMEM Glutamax (Dulbecco) containing 10% fetal calf serum (Invitrogen, Carlsbad, CA), 100 μg of penicillin/ml and 100 μg streptomycin/ml (Invitrogen). U2OS cells used for NF-κB-luciferase reporter assays were maintained in DMEM Glutamax (Dulbecco) containing 5% dextran-coated charcoal stripped fetal calf serum (67) (Invitrogen), 100 μg of penicillin/ml and 100 μg streptomycin/ml (Invitrogen). The murine NIH-3T3 cell line was cultured in the same media but now with 10% bovine serum (Invitrogen), 100 μg of penicillin/ml, and 100 μg streptomycin/ml (Invitrogen). For luciferase reporter assays, cells were seeded in 24-well plates and transiently transfected using the calcium-phosphate precipitation method. Each well was cotransfected with a reporter construct, PPAR expression constructs and 2 ng pCMV-Renilla (Promega, Madison, WI) or 12.5 ng TK-Renilla (Promega) as indicated in the figure legends. The next day, cells were washed twice with HBS (pH 7.05) and subsequently maintained in medium in absence or presence of PPAR ligands for 24 h. After incubation, cells were washed twice with PBS and harvested in passive lysisbuffer (Promega) and assayed for luciferase activity according to the manufacturer's protocol (Promega Dual-Luciferase Reporter Assay System) and for *Renilla* luciferase activity to correct for transfection efficiency. The relative light units were measured by a Centro LB 960 luminometer (Berthold Technologies, Bad Wildbad, Germany).

For Western blot analyses of the different PPARγ proteins, U2OS cells were transiently transfected with 2 μg PPARγ

expression construct using Fugene 6 transfection reagent and treated as described as above. Cells were lysed in Laemmli sample buffer and subjected to SDS-PAGE and transferred to Immobilon membranes (Millipore, Eugene, OR). α-PPARγ antibody was used to probe for PPARγ protein and ECL (Amersham Biosciences, Arlington Heights, IL) was used for detection.

### GST Pull-Downs

Recombinant PPARγ2 cDNAs (wild type or mutants) in the pCDNA3 expression vector were transcribed and translated *in vitro* in reticulolysate in the presence of [$^{35}$S]methionine according to manufacturer's protocol (TNT T7 Quick Coupled Transcription/Translation Kit; Promega). Rosetta pLysS competent bacteria (Novagen, Madison, WI) were transformed with GST expression plasmids. GST fusion proteins were induced and purified as described earlier (62). [$^{35}$S]-labeled proteins were incubated with GST fusion proteins in NETN buffer [20 mM Tris (pH 8.0), 100 mM NaCl, 1 mM EDTA, 0.5% Nonidet P-40) containing protease inhibitors (Complete; Roche Applied Biosciences). Samples were subsequently washed and subjected to SDS-PAGE. Gels were enhanced with Amplify (Amersham) and dried and the [$^{35}$S]-labeled proteins were visualized by fluorography. For each assay, at least three independent pull downs were performed.

### EMSA

Double-stranded DNA oligomers, containing the PPRE from the rat acyltransferase-coenzyme A oxidase promoter (36), were labeled with [α-$^{32}$P]deoxy-ATP using Klenow enzyme and purified using Probe Quant G-50 Micro Colums (Amersham Biosciences). *In vitro*-translated PPARγ (wild type or mutants) and/or *in vitro*-translated RXRα proteins were preincubated for 15 min at room temperature in absence or presence of 10-fold cold probe (wild type or mutant) in a buffer containing 10 μg BSA, 1 μg poly deoyinosine:deoxycytosine, 40 mM HEPES (pH 7.4), 100 mM KCl, 2 mM dithiothreitol and 20% glycerol. For supershift experiments 1 μg of α-RXR or α-PPARγ or α-Gal4 antibodies were added to the preincubation mix. After preincubation, purified [$^{32}$P]-labeled probe was added and incubated for 30 min at room temperature, followed by 30 min at 4 C. Receptor-DNA complexes were separated from unbound DNA on nondenaturing polyacrylamide gels and visualized by autoradiography. At least three independent experiments were performed.

The complete probe sequences used for binding and competition analysis were as follows: PPRE-wild-type, 5′-CCGGGGACCAGGACAAAGGTCACGAAGCT-3′ and PPRE-mutant, 5′-CCGGGGGACCAGCACAAAGCACACGAAGCT-3′.

### Ligand-Binding Assay

Filter binding assays were performed as described by Adams *et al.* (68) with minor modifications. Bacterially expressed and purified GST-PPARγ2 fusion proteins were incubated with 10 or 100 nM [$^{3}$H]-rosiglitazone in binding buffer [50 mM HEPES (pH 7.9), 100 mM KCl, 2 mM dithiothreitol, 10% glycerol) followed by incubation with an 200-fold excess of competing cold ligand (rosiglitazone). Bound ligand was separated from unbound ligand by passage through a filter membrane (Millipore HA filters; 0.45 mm) under vacuum followed by three washes with binding buffer. Filters were then transferred into tubes containing scintillation fluid and counted in a γ-counter. Binding experiments were performed independently three times.

### Differentiation Assay

Retrovirus was produced by Fugene transfection of Phoenix Ampho cells with the parental retroviral pMSCV-vector, pMSCV containing either wild-type murine PPARγ2, or PPARγ2 R425C and collection of virus supernatants. NIH-3T3 fibroblasts were infected overnight with the virus supernatants in medium containing 4 μg/ml polybrene and infected cells were selected by addition of 2 μg/ml puromycine to the culture medium. Selected cells were grown to confluency and after 2 d incubated with culture medium containing dexamethasone (250 nM), 3-isobutyl-1-methylxanthine (500 μM), insulin (170 nM), and rosiglitazone (2.5 nM) for 2 d. At d 3, medium was changed for culture medium supplemented with insulin (170 nM) and rosiglitazone (2.5 nM) and left for a week. Cells were subsequently washed and triglycerides were stained by Oil-Red-O and the cell nuclei by crystal violet. Stained cells were photographed with a light microscope (Zeiss Axiovert 40 CFL; Carl Zeiss, Jena, Germany) coupled to a digital camera (Canon DSC Powershot G5; Canon, Tokyo, Japan). Two independent retroviral transductions were performed.

For Western blot analyses, differentiated NIH-3T3 cell lines (empty vector, PPARγ wild type, or PPARγ2 R425C) were lysed in Laemmli sample buffer and samples were subjected to SDS-PAGE and transferred to Immobilon membranes (Millipore). α-PPARγ and α-tropomyosin antibodies were used to probe for PPARγ protein and tropomyosin protein respectively. ECL (Amersham Biosciences) was used for detection.

### Quantitative RT-PCR

Transduced NIH-3T3 fibroblasts were differentiated as described above. For each cell line (empty vector, PPARγ2 wild type, or PPARγ2 R425C), total RNA from three wells was isolated independently using TriPure reagent (Roche Applied Science) and reverse-transcribed using Moloney murine leukemia virus-reverse transcriptase ribonuclease H Minus Point Mutant (Promega), according to manufacturer's protocol. Transcription levels were determined by real-time PCR using the LightCycler (Roche Applied Science). Briefly, the relative expression of the housekeeping gene *Hprt1* (hypoxanthine-guanine phosphoribosyltransferase 1) was used to calculate the relative expression level of the PPARγ2 target genes *Fabp4*, *Aqp7* and *Gyk* respectively, according to Vandesompele *et al.* (69). The PCRs were performed using the DNA Master SYBR-green 1 kit (Roche Applied Science) and contained 5.0 μl 1:40 diluted cDNA, 0.25 pmol/μl primer, DNA master SYBR-green I solution, and $MgCl_2$ (3.5 mM). Reactions were carried out in triplicate for each sample.

The sequences of the primers are as follows: murine *Hprt1* sense primer; 5′-TCCTCCTCAGACCGCTTTT-3′; antisense primer, 5′-CCTGGTTCATCATCGCTAATC-3′; murine *Fabp4* sense primer 5′-GAAAACGAGATGGTGACAAGC-3′; antisense primer 5′-TTGTGGAAGTCACGCCTTT-3′; murine *Aqp7* sense primer, 5′ GGCTTCTCCCTTCCTCTAGTTT-3′; antisense primer, 5′- AAGGCCACTGAGGAAGTCATT-3′; murine *Gyk* sense primer, 5′-TTCCAGGAAATAATAACTTTGTCAAG-3′; antisense primer, 5′-CACTGCACTGAAATACGTGCT-3′.

### Molecular Dynamics Simulations

Molecular dynamics simulations were performed with the GROMACS 3.1.4 package (70, 71), using the GROMOS96 43A1 force field (72). The starting structure of the wild-type protein was obtained from the protein data bank (73), entry 1FM6 (16), chain D or chain X and entry 1FM9 chain D; the mutant protein structure was obtained by replacing arginine 425 by a cysteine (for 1FM6 chain D) or by an alanine (for all three chains). Cofactors and ligands were removed. Each simulation was run for 5.0 nsec. A total of seven simulations was thus performed: three for wild type, three for the R425A mutant, and one for the R425C mutant.

The starting structure was solvated in a cubic box with a minimum solute-box distance of 14Å, filled with approximately

25,000 single point charge water molecules (74) and 5 (wild type) or 6 (mutant) additional $Na^+$ ions to electro-neutralize the system, respectively. Periodic boundary conditions were applied.

Each system was first energy minimized using 1.000 steps of Steepest Descent algorithm. After this, equilibration was performed in five 20-psec phases during which the force constant of the position restraints term for the solute was decreased from 1000 to 0 KJ $mol^{-1}$ $nm^{-2}$ (1000, 1000, 100, 10, and 0 KJ $mol^{-1}$ $nm^{-2}$, respectively). The initial velocities were generated at 300K following a Maxwellian distribution.

Solute, solvent, and counterions were independently weakly coupled to reference temperature baths at 300 K ($\tau$ = 0.1 psec) (75). The pressure was maintained by weakly coupling the system to an external pressure bath at one atmosphere except for the first 20 psec equilibration part, which was performed at constant volume [NVT: constant number of particles (N), volume (V) and temperature (T)]. The LINCS algorithm (76) was used to constrain bond lengths, allowing an integration time step of 0.002 psec (2 fsec) to be used. The nonbonded interactions were calculated with a twin-range cutoff (77) of 0.8 and 1.4 nm. The long-range electrostatic interactions beyond the 1.4 nm cutoff were treated with the generalized reaction field model (78) using a dielectric constant of 54. The nonbonded interaction pair list was updated every five steps. Trajectory coordinates and energies were stored at 0.5-psec intervals. The analysis was performed using the set of programs within GROMACS. Figures were generated using MolScript (79) and Raster3D (80).

## Acknowledgments

We thank Drs. S. Ali, J. D. Baxter, E. Burstein, V. K. K. Chatterjee, R. M. Evans, M. Gurnell, N. Maeda, M. G. Parker, B. M. Spiegelman, and R. G. Roeder for various plasmid constructs. We would also like to thank Drs. J. M. Stephens, G. E. Folkers, P. Muller, and M. Agostini for helpful suggestions and Drs. D. A. Baker, P. J. Coffer, L. W. Klomp and M. G. Parker for critical reading of the manuscript.

Received November 21, 2006. Accepted February 13, 2007.

Address all correspondence and requests for reprints to: Eric Kalkhoven, Department of Metabolic and Endocrine Diseases, University Medical Center Utrecht, Room KE.03.139.2, Lundlaan 6, 3584 EA Utrecht, The Netherlands. E-mail: e.kalkhoven@umcutrecht.nl.

This work was supported by a fellowship from the Royal Netherlands Academy of Arts and Sciences (to E.K.) and by a Jonge Chemici grant (Grant No. 700.50.512) from the Netherlands Organization for Scientific Research (to A.M.J.J.B.).

Disclosure Statement: The authors have nothing to disclose.

## REFERENCES

1. Friedman JM 2003 A war on obesity, not the obese. Science 299:856–858
2. Simha V, Garg A 2006 Lipodystrophy: lessons in lipid and energy metabolism. Curr Opin Lipidol 17:162–169
3. Capeau J, Magre J, Lascols O, Caron M, Bereziat V, Vigouroux C, Bastard JP 2005 Diseases of adipose tissue: genetic and acquired lipodystrophies. Biochem Soc Trans 33:1073–1077
4. Garg A 2004 Acquired and inherited lipodystrophies. N Engl J Med 350:1220–1234
5. Nolan D, Mallal S 2004 Complications associated with NRTI therapy: update on clinical features and possible pathogenic mechanisms. Antivir Ther 9:849–863
6. Semple RK, Chatterjee VK, O'Rahilly S 2006 PPARγ and human metabolic disease. J Clin Invest 116:581–589
7. Hegele RA 2005 Lessons from human mutations in PPARgamma. Int J Obes (Lond) 29(Suppl 1):S31–S35
8. Willson TM, Brown PJ, Sternbach DD, Henke BR 2000 The PPARs: from orphan receptors to drug discovery. J Med Chem 43:527–550
9. Lehrke M, Lazar MA 2005 The many faces of PPARγ. Cell 123:993–999
10. Feige JN, Gelman L, Michalik L, Desvergne B, Wahli W 2006 From molecular action to physiological outputs: peroxisome proliferator-activated receptors are nuclear receptors at the crossroads of key cellular functions. Prog Lipid Res 45:120–159
11. Tontonoz P, Hu E, Spiegelman BM 1994 Stimulation of adipogenesis in fibroblasts by PPARγ2, a lipid-activated transcription factor. Cell 79:1147–1156
12. Barak Y, Nelson MC, Ong ES, Jones YZ, Ruiz-Lozano P, Chien KR, Koder A, Evans RM 1999 PPARγ is required for placental, cardiac, and adipose tissue development. Mol Cell 4:585–595
13. Kubota N, Terauchi Y, Miki H, Tamemoto H, Yamauchi T, Komeda K, Satoh S, Nakano R, Ishii C, Sugiyama T, Eto K, Tsubamoto Y, Okuno A, Murakami K, Sekihara H, Hasegawa G, Naito M, Toyoshima Y, Tanaka S, Shiota K, Kitamura T, Fujita T, Ezaki O, Aizawa S, Kadowaki T 1999 PPARγ mediates high-fat diet-induced adipocyte hypertrophy and insulin resistance. Mol Cell 4:597–609
14. Rosen ED, Sarraf P, Troy AE, Bradwin G, Moore K, Milstone DS, Spiegelman BM, Mortensen RM 1999 PPARγ is required for the differentiation of adipose tissue in vivo and in vitro. Mol Cell 4:611–617
15. Evans RM, Barish GD, Wang YX 2004 PPARs and the complex journey to obesity. Nat Med 10:355–361
16. Gampe Jr RT, Montana VG, Lambert MH, Miller AB, Bledsoe RK, Milburn MV, Kliewer SA, Willson TM, Xu HE 2000 Asymmetry in the PPARγ/RXRα crystal structure reveals the molecular basis of heterodimerization among nuclear receptors. Mol Cell 5:545–555
17. Nolte RT, Wisely GB, Westin S, Cobb JE, Lambert MH, Kurokawa R, Rosenfeld MG, Willson TM, Glass CK, Milburn MV 1998 Ligand binding and co-activator assembly of the peroxisome proliferator-activated receptor-γ. Nature 395:137–143
18. Yu C, Markan K, Temple KA, Deplewski D, Brady MJ, Cohen RN 2005 The nuclear receptor corepressors NCoR and SMRT decrease peroxisome proliferator-activated receptor γ transcriptional activity and repress 3T3–L1 adipogenesis. J Biol Chem 280:13600–13605
19. Guan HP, Ishizuka T, Chui PC, Lehrke M, Lazar MA 2005 Corepressors selectively control the transcriptional activity of PPARγ in adipocytes. Genes Dev 19:453–461
20. Chui PC, Guan HP, Lehrke M, Lazar MA 2005 PPARγ regulates adipocyte cholesterol metabolism via oxidized LDL receptor 1. J Clin Invest 115:2244–2256
21. Westin S, Kurokawa R, Nolte RT, Wisely GB, McInerney EM, Rose DW, Milburn MV, Rosenfeld MG, Glass CK 1998 Interactions controlling the assembly of nuclear-receptor heterodimers and co-activators. Nature 395: 199–202
22. Perissi V, Rosenfeld MG 2005 Controlling nuclear receptors: the circular logic of cofactor cycles. Nat Rev Mol Cell Biol 6:542–554
23. Forman BM, Tontonoz P, Chen J, Brun RP, Spiegelman BM, Evans RM 1995 15-Deoxy-δ12, 14-prostaglandin J2 is a ligand for the adipocyte determination factor PPARγ. Cell 83:803–812
24. Krey G, Braissant O, L'Horset F, Kalkhoven E, Perroud M, Parker MG, Wahli W 1997 Fatty acids, eicosanoids, and hypolipidemic agents identified as ligands of peroxisome proliferator-activated receptors by coactivator-dependent receptor ligand assay. Mol Endocrinol 11: 779–791

25. Lehmann JM, Moore LB, Smith-Oliver TA, Wilkison WO, Willson TM, Kliewer SA 1995 An antidiabetic thiazolidinedione is a high affinity ligand for peroxisome proliferator-activated receptor γ (PPARγ). J Biol Chem 270: 12953–12956
26. Henke BR, Blanchard SG, Brackeen MF, Brown KK, Cobb JE, Collins JL, Harrington Jr WW, Hashim MA, Hull-Ryde EA, Kaldor I, Kliewer SA, Lake DH, Leesnitzer LM, Lehmann JM, Lenhard JM, Orband-Miller LA, Miller JF, Mook Jr RA, Noble SA, Oliver Jr W, Parks DJ, Plunket KD, Szewczyk JR, Willson TM 1998 N-(2-benzoylphenyl)-L-tyrosine PPARγ agonists. 1. Discovery of a novel series of potent antihyperglycemic and antihyperlipidemic agents. J Med Chem 41:5020–5036
27. Sethi JK, Hotamisligil GS 1999 The role of TNFα in adipocyte metabolism. Semin Cell Dev Biol 10:19–29
28. Ruan H, Lodish HF 2003 Insulin resistance in adipose tissue: direct and indirect effects of tumor necrosis factor-α. Cytokine Growth Factor Rev 14:447–455
29. Barroso I, Gurnell M, Crowley VE, Agostini M, Schwabe JW, Soos MA, Maslen GL, Williams TD, Lewis H, Schafer AJ, Chatterjee VK, O'Rahilly S 1999 Dominant negative mutations in human PPARγ associated with severe insulin resistance, diabetes mellitus and hypertension. Nature 402:880–883
30. Hegele RA, Cao H, Frankowski C, Mathews ST, Leff T 2002 PPARG F388L, a transactivation-deficient mutant, in familial partial lipodystrophy. Diabetes 51:3586–3590
31. Agarwal AK, Garg A 2002 A novel heterozygous mutation in peroxisome proliferator-activated receptor-γ gene in a patient with familial partial lipodystrophy. J Clin Endocrinol Metab 87:408–411
32. Agostini M, Schoenmakers E, Mitchell C, Szatmari I, Savage D, Smith A, Rajanayagam O, Semple R, Luan J, Bath L, Zalin A, Labib M, Kumar S, Simpson H, Blom D, Marais D, Schwabe J, Barroso I, Trembath R, Wareham N, Nagy L, Gurnell M, O'Rahilly S, Chatterjee K 2006 Non-DNA binding, dominant-negative, human PPARγ mutations cause lipodystrophic insulin resistance. Cell Metab 4:303–311
33. Francis GA, Li G, Casey R, Wang J, Cao H, Leff T, Hegele RA 2006 Peroxisomal proliferator activated receptor-γ deficiency in a Canadian kindred with familial partial lipodystrophy type 3 (FPLD3). BMC Med Genet 7:3
34. Savage DB, Agostini M, Barroso I, Gurnell M, Luan J, Meirhaeghe A, Harding AH, Ihrke G, Rajanayagam O, Soos MA, George S, Berger D, Thomas EL, Bell JD, Meeran K, Ross RJ, Vidal-Puig A, Wareham NJ, O'Rahilly S, Chatterjee VK, Schafer AJ 2002 Digenic inheritance of severe insulin resistance in a human pedigree. Nat Genet 31:379–384
35. Brelivet Y, Kammerer S, Rochel N, Poch O, Moras D 2004 Signature of the oligomeric behaviour of nuclear receptors at the sequence and structural level. EMBO Rep 5:423–429
36. Tugwood JD, Issemann I, Anderson RG, Bundell KR, McPheat WL, Green S 1992 The mouse peroxisome proliferator activated receptor recognizes a response element in the 5′ flanking sequence of the rat acyl CoA oxidase gene. EMBO J 11:433–439
37. Agostini M, Gurnell M, Savage DB, Wood EM, Smith AG, Rajanayagam O, Garnes KT, Levinson SH, Xu HE, Schwabe JW, Willson TM, O'Rahilly S, Chatterjee VK 2004 Tyrosine agonists reverse the molecular defects associated with dominant-negative mutations in human peroxisome proliferator-activated receptor γ. Endocrinology 145:1527–1538
38. Kondo H, Shimomura I, Kishida K, Kuriyama H, Makino Y, Nishizawa H, Matsuda M, Maeda N, Nagaretani H, Kihara S, Kurachi Y, Nakamura T, Funahashi T, Matsuzawa Y 2002 Human aquaporin adipose (AQPap) gene. Genomic structure, promoter analysis and functional mutation. Eur J Biochem 269:1814–1826
39. Molnar F, Matilainen M, Carlberg C 2005 Structural determinants of the agonist-independent association of human peroxisome proliferator-activated receptors with coactivators. J Biol Chem 280:26543–26556
40. Yen PM 2003 Molecular basis of resistance to thyroid hormone. Trends Endocrinol Metab 14:327–333
41. Clifton-Bligh RJ, de Zegher F, Wagner RL, Collingwood TN, Francois I, Van Helvoirt M, Fletterick RJ, Chatterjee VK 1998 A novel TR beta mutation (R383H) in resistance to thyroid hormone syndrome predominantly impairs corepressor release and negative transcriptional regulation. Mol Endocrinol 12:609–621
42. Fawell SE, Lees JA, White R, Parker MG 1990 Characterization and colocalization of steroid binding and dimerization activities in the mouse estrogen receptor. Cell 60:953–962
43. Chen S, Johnson BA, Li Y, Aster S, McKeever B, Mosley R, Moller DE, Zhou G 2000 Both coactivator LXXLL motif-dependent and -independent interactions are required for peroxisome proliferator-activated receptor γ (PPARγ) function. J Biol Chem 275:3733–3736
44. Schulman IG, Shao G, Heyman RA 1998 Transactivation by retinoid X receptor-peroxisome proliferator-activated receptor γ (PPARγ) heterodimers: intermolecular synergy requires only the PPARγ hormone-dependent activation function. Mol Cell Biol 18:3483–3494
45. Gelman L, Zhou G, Fajas L, Raspe E, Fruchart JC, Auwerx J 1999 p300 interacts with the N- and C-terminal part of PPARγ2 in a ligand-independent and -dependent manner, respectively. J Biol Chem 274:7681–7688
46. Heck S, Bender K, Kullmann M, Gottlicher M, Herrlich P, Cato AC 1997 IκBα-independent downregulation of NF-κB activity by glucocorticoid receptor. EMBO J 16: 4698–4707
47. Suzawa M, Takada I, Yanagisawa J, Ohtake F, Ogawa S, Yamauchi T, Kadowaki T, Takeuchi Y, Shibuya H, Gotoh Y, Matsumoto K, Kato S 2003 Cytokines suppress adipogenesis and PPAR-γ function through the TAK1/TAB1/NIK cascade. Nat Cell Biol 5:224–230
48. Gurnell M, Wentworth JM, Agostini M, Adams M, Collingwood TN, Provenzano C, Browne PO, Rajanayagam O, Burris TP, Schwabe JW, Lazar MA, Chatterjee VK 2000 A dominant-negative peroxisome proliferator-activated receptor γ (PPARγ) mutant is a constitutive repressor and inhibits PPARγ-mediated adipogenesis. J Biol Chem 275:5754–5759
49. Pascual G, Fong AL, Ogawa S, Gamliel A, Li AC, Perissi V, Rose DW, Willson TM, Rosenfeld MG, Glass CK 2005 A SUMOylation-dependent pathway mediates transrepression of inflammatory response genes by PPAR-γ. Nature 437:759–763
50. Xu HE, Stanley TB, Montana VG, Lambert MH, Shearer BG, Cobb JE, McKee DD, Galardi CM, Plunket KD, Nolte RT, Parks DJ, Moore JT, Kliewer SA, Willson TM, Stimmel JB 2002 Structural basis for antagonist-mediated recruitment of nuclear co-repressors by PPARα. Nature 415:813–817
51. Vaisanen S, Duchier C, Rouvinen J, Maenpaa PH 1999 The importance of the putative helices 4 and 5 of human vitamin D(3) receptor for conformation and ligand binding. Biochem Biophys Res Commun 264:478–482
52. Vivat-Hannah V, Bourguet W, Gottardis M, Gronemeyer H 2003 Separation of retinoid X receptor homo- and heterodimerization functions. Mol Cell Biol 23: 7678–7688
53. Collingwood TN, Adams M, Tone Y, Chatterjee VK 1994 Spectrum of transcriptional, dimerization, and dominant negative properties of twenty different mutant thyroid hormone β-receptors in thyroid hormone resistance syndrome. Mol Endocrinol 8:1262–1277
54. Nagaya T, Jameson JL 1993 Thyroid hormone receptor dimerization is required for dominant negative inhibition

by mutations that cause thyroid hormone resistance. J Biol Chem 268:15766–15771
55. Al Shali K, Cao H, Knoers N, Hermus AR, Tack CJ, Hegele RA 2004 A single-base mutation in the peroxisome proliferator-activated receptor γ4 promoter associated with altered *in vitro* expression and partial lipodystrophy. J Clin Endocrinol Metab 89:5655–5660
56. Tsai YS, Maeda N 2005 PPARγ: a critical determinant of body fat distribution in humans and mice. Trends Cardiovasc Med 15:81–85
57. Gray SL, Dalla NE, Vidal-Puig AJ 2005 Mouse models of PPAR-γ deficiency: dissecting PPAR-γ's role in metabolic homoeostasis. Biochem Soc Trans 33:1053–1058
58. Ausubel FM, Brent R, Kingston R, Moore D, Seidman JJ, Smith J, Struhl K 1993 Current protocols in molecular biology. New York: John Wiley & Sons
59. Burstein E, Hoberg JE, Wilkinson AS, Rumble JM, Csomos RA, Komarck CM, Maine GN, Wilkinson JC, Mayo MW, Duckett CS 2005 COMMD proteins, a novel family of structural and functional homologs of MURR1. J Biol Chem 280:22222–22232
60. Ge K, Guermah M, Yuan CX, Ito M, Wallberg AE, Spiegelman BM, Roeder RG 2002 Transcription coactivator TRAP220 is required for PPARγ2-stimulated adipogenesis. Nature 417:563–567
61. Chen JD, Evans RM 1995 A transcriptional co-repressor that interacts with nuclear hormone receptors. Nature 377:454–457
62. Kalkhoven E, Valentine JE, Heery DM, Parker MG 1998 Isoforms of steroid receptor co-activator 1 differ in their ability to potentiate transcription by the oestrogen receptor. EMBO J 17:232–243
63. Wissink S, van Heerde EC, Schmitz ML, Kalkhoven E, van der BB, Baeuerle PA, van der Saag PT 1997 Distinct domains of the RelA NF-κB subunit are required for negative cross-talk and direct interaction with the glucocorticoid receptor. J Biol Chem 272:22278–22284
64. Kalkhoven E, Teunissen H, Houweling A, Verrijzer CP, Zantema A 2002 The PHD type zinc finger is an integral part of the CBP acetyltransferase domain. Mol Cell Biol 22:1961–1970
65. Ribeiro RC, Feng W, Wagner RL, Costa CH, Pereira AC, Apriletti JW, Fletterick RJ, Baxter JD 2001 Definition of the surface in the thyroid hormone receptor ligand binding domain for association as homodimers and heterodimers with retinoid X receptor. J Biol Chem 276: 14987–14995
66. Butler AJ, Parker MG 1995 COUP-TF II homodimers are formed in preference to heterodimers with RXRα or TRβ in intact cells. Nucleic Acids Res 23:4143–4150
67. van der BB, Rutteman GR, Blankenstein MA, de Laat SW, van Zoelen EJ 1988 Mitogenic stimulation of human breast cancer cells in a growth factor-defined medium: synergistic action of insulin and estrogen. J Cell Physiol 134:101–108
68. Adams M, Matthews C, Collingwood TN, Tone Y, Beck-Peccoz P, Chatterjee KK 1994 Genetic analysis of 29 kindreds with generalized and pituitary resistance to thyroid hormone. Identification of thirteen novel mutations in the thyroid hormone receptor β gene. J Clin Invest 94: 506–515
69. Vandesompele J, De Preter K, Pattyn F, Poppe B, Van Roy N, De Paepe A, Speleman F 2002 Accurate normalization of real-time quantitative RT-PCR data by geometric averaging of multiple internal control genes. Genome Biol 3:RESEARCH0034
70. Lindahl E, Hess B, van der Spoel D 2001 GROMACS 3.0: a package for molecular simulation and trajectory analysis. J Mol Model 7:306–317
71. Berendsen HJC, Vanderspoel D, Vandrunen R 1995 Gromacs—a message-passing parallel molecular-dynamics implementation. Comp Phys Commun 91:43–56
72. Daura X, Jaun B, Seebach D, van Gunsteren WF, Mark AE 1998 Reversible peptide folding in solution by molecular dynamics simulation. J Mol Biol 280:925–932
73. Berman HM, Westbrook J, Feng Z, Gilliland G, Bhat TN, Weissig H, Shindyalov IN, Bourne PE 2000 The Protein Data Bank. Nucleic Acids Res 28:235–242
74. Berendsen HJC, Postma JPM, van Gunsteren WF 1981 Interaction models for water in relation to protein hydration. In: Pullman B, ed. Intermolecular forces. Dordrecht, The Netherlands: Reidel; 331–342
75. Berendsen HJC, Postma JPM, van Gunsteren WF, DiNola A, Haak JR 1984 Molecular dynamics with coupling to an external bath. J Chem Phys 81:3684–3690
76. Hess B, Bekker H, Berendsen HJC, Fraaije JGEM 1997 LINCS: a linear constraint solver for molecular simulations. J Comput Chem 18:1463–1472
77. Vangunsteren WF, Berendsen HJC 1990 Computer-simulation of molecular-dynamics—methodology, applications, and perspectives in chemistry. Angewandte Chemie (International Edition in English) 29:992–1023
78. Tironi IG, Sperb R, Smith PE, Vangunsteren WF 1995 A generalized reaction field method for molecular-dynamics simulations. J Chem Phys 102:5451–5459
79. Kraulis PJ 1991 MolScript—a program to produce both detailed and schematic plots of protein structures. J Appl Crystallogr 24:946–950
80. Merritt EA, Murphy MEP 1994 Raster3D Version 2.0—a program for photorealistic molecular graphics. Acta Crystallogr D 50:869–873

***Molecular Endocrinology*** **is published monthly by The Endocrine Society (http://www.endo-society.org), the foremost professional society serving the endocrine community.**